Direct Model Predictive Control of Bidirectional Quasi-Z-Source Inverters Fed PMSM Drives

Ayman Ayad*, Petros Karamanakos†, Ralph Kennel*, and José Rodríguez**
* Chair of Electrical Drive Systems and Power Electronics, Technische Universität München, Munich, Germany
† Department of Electrical Engineering, Tampere University of Technology, Tampere, Finland
** Universidad Nacional Andrés Bello, Santiago, Chile
Email: ayman.francees@tum.de, p.karamanakos@ieee.org, ralph.kennel@tum.de, jose.rodriguez@unab.cl

***Abstract*—This paper proposes a direct model predictive control (MPC) strategy to control the bidirectional quasi-Z-source inverter (BqZSI) driving a permanent magnet synchronous machine (PMSM) for electric vehicle applications. The dq machine currents are simultaneously controlled with the capacitor voltage and inductor current of the dc side. The physical model of the BqZSI with PMSM is first derived which encompasses different operating modes and states of the BqZSI. To examine the performance of the proposed control scheme at steady-state and transient operation, simulations based on MATLAB/Simulink are conducted. The results indicate that the proposed control scheme offers a very good steady-state performance as well as fast dynamic responses during transients.**

I. Introduction

The increasing concern about global environmental problems has contributed to increase the attention towards electric vehicles (EVs). For EVs, the induction machines (IMs) and permanent magnet synchronous machines (PMSMs) are the most commonly used machines. However, the PMSM is always preferred as it brings higher power density, efficiency, and reliability [1], [2].

Regardless of the machine type, batteries are used as the main source. By using voltage source inverters (VSIs), the dc current is converted to ac in order to feed the EV machine. However, the dc-link voltage can not be controlled over a wide speed range. To solve this problem, the flux weakening technique is utilized in high speed which results in lower efficiency. To control the dc-link voltage, a dc-dc converter is combined with the VSI. Although the additional converter increases the traction system efficiency, it also increases the cost and the controller complexity [3].

In 2002, the Z-source inverter (ZSI) was proposed as an alternative to the conventional two-stage inverter [4]. The ZSI is considered as a single-stage buck-boost inverter. It uses an impedance Z-network and includes an extra switching state, defined as shoot-through state. Based on this impedance network, the input dc voltage can be boosted to the required dc-link voltage level. Thus, the ZSI is consider as an attractive solution for EV applications as the dc-link voltage can be adjusted such that the machine can work above the rated speed without a need for a filed weakening strategy. This in turn decreases the machine losses and increases the system efficiency [5].

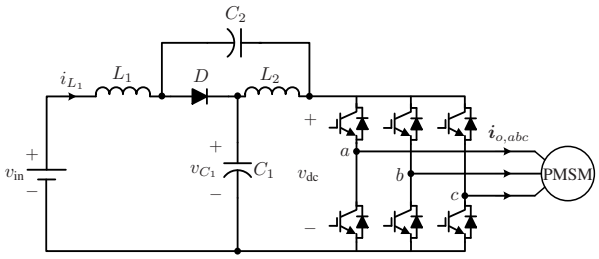

Fig. 1: The classical quasi-Z-source inverter (qZSI) topology.

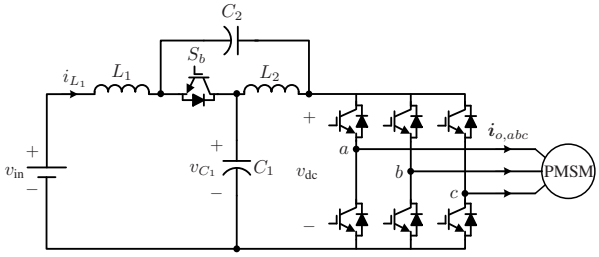

Fig. 2: The bidirectional quasi-Z-source inverter (BqZSI) topology.

Later, the quasi-Z-source inverter (qZSI) [6], modified version of the ZSI, was proposed and widely used with different applications [7]. Compared to the ZSI, the qZSI draws a continuous input current, requires smaller passive components, and provides a common earthing between the input dc voltage and the dc-link bus [8]. In order to comply with the requirements of the EV application, a bidirectional qZSI (BqZSI) is used by replacing the diode in the qZS network by an IGBT switch [3], [9], [10], see Figs. 1 and 2.

For the examined application, there are a few papers in the literature focusing on the control of BqZSI feeding a PMSM, e.g. [3], [5], [9], [10]. In [5], [10], the conventional proportional-integral (PI) controllers are used to regulate the system variables on both sides of the bidirectional ZSI/qZSI; the inductor current and/or capacitor voltage on the dc side and the output dq currents (based on reference speed/torque) on the machine side. Moreover, a control method based on the flatness properties of the system is proposed in [3]. Although these control schemes introduce satisfying performances, their design and tuning are still challenging.

In recent years, direct model predictive control (MPC) has been established as an effective control strategy for a wide range of power electronics applications [11], [12]. MPC can handle multiple—and usually competing—control objectives,

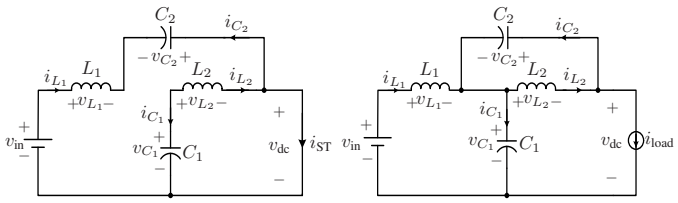

(a) Shoot-through state. (b) Non-shoot-through state.

Fig. 3: Operation states of the qZSI during the boost mode.

can deal with nonlinearities and complex dynamics as well as it shows fast dynamic responses [11]. Thanks to these advantages, MPC has been applied to PMSM drives combined with different power electronic converters as a current and/or torque controller, see [13]–[15]. In addition, more recent works have been published on MPC for the qZSI connected with an RL load [16], [17]. In [18], a predictive torque control scheme of an IM fed by a BqZSI is presented. Nevertheless, MPC as a current controller with BqZSI fed PMSM drives has not been examined yet.

This paper proposes an MPC strategy that controls both sides of the BqZSI connected with a PMSM for EV applications. The main control variable on the machine side is the machine current, i.e. the dq currents should be regulated along their reference values (computed from an outer control loop). In addition, the dc-side variables, namely the capacitor voltage and inductor current, should track their reference trajectories in order to adjust the dc-link voltage to a desired level over a wide speed range. Moreover, the switching frequency is to be controlled by penalizing the switching transitions. The overall model of the system is derived and the control strategy is proposed. To evaluate the system performance with MPC, simulation results are presented and discussed.

II. System Mathematical Model

The system under investigation is shown in Fig. 2. It combines a BqZS network with a two-level three-phase VSI and a PMSM drive. The BqZSI can operate in two modes, namely boost and buck mode, see Fig. 3. In boost mode, it utilizes the shoot-through switching state combined with the non-shoot-through states in order to boost the input dc voltage to the desired dc-link level. On the other hand, in buck mode, the BqZSI acts as the conventional VSI, where the dc-link voltage approximately equals to the input dc voltage. Note that the switch S_b is inserted instead of the diode D in order to allow a bidirectional power flow [5]. The full model of the proposed system can be divided into two models; dc-side and machine-side model.

A. Dc-Side Model

As mentioned above, BqZSI in boost mode has two different switching states; shoot-through and non-shoot-through state. The models of both cases will be separately derived and then combined in one model at the end.

1) Shoot-Through state: As can be noted in Fig. 3(a), when at least one of the three phases of the inverter is short circuited, the diode of the switch S_b is cut off. Note that the firing signal of the switch S_b is the complement of the shoot-through signal . Hence, the capacitors charge the inductors and the system model is given by

$$\frac{\mathrm{d}i_{L_1}(t)}{\mathrm{d}t} = \frac{1}{L_1}v_{C_2} + \frac{1}{L_1}v_{\text{in}}\,, \quad \frac{\mathrm{d}i_{L_2}(t)}{\mathrm{d}t} = \frac{1}{L_2}v_{C_1}\,, \tag{1a}$$

$$\frac{\mathrm{d}v_{C_1}(t)}{\mathrm{d}t} = \frac{1}{C_1}i_{L_2}\,, \quad \frac{\mathrm{d}v_{C_2}(t)}{\mathrm{d}t} = \frac{1}{C_2}i_{L_1}\,, \tag{1b}$$

where L_1, L_2 and C_1, C_2 are the inductances and capacitances of the qZS network.

2) Non-Shoot-Through state: During the non-shoot-through state, as shown in Fig. 3(b), the input dc source and the inductors charge the capacitors and provide energy to the machine. Consequently, the system model can be written as

$$\frac{\mathrm{d}i_{L_1}(t)}{\mathrm{d}t} = -\frac{1}{L_1}v_{C_1} + \frac{1}{L_1}v_{\text{in}}, \quad \frac{\mathrm{d}i_{L_2}(t)}{\mathrm{d}t} = -\frac{1}{L_2}v_{C_2}\,, \tag{2a}$$

$$\frac{\mathrm{d}v_{C_1}(t)}{\mathrm{d}t} = \frac{1}{C_1}i_{L_1} - \frac{1}{C_1}i_{\text{load}}, \quad \frac{\mathrm{d}v_{C_2}(t)}{\mathrm{d}t} = \frac{1}{C_2}i_{L_2} - \frac{1}{C_2}i_{\text{load}} \tag{2b}$$

where i_{load} denotes the dc current drawn by the inverter during non-shoot-through states.

B. Machine-side Model

In the synchronous rotating dq frame, the differential stator current equations of the PMSM can be written as

$$\frac{\mathrm{d}i_{o,d}(t)}{\mathrm{d}t} = -\frac{R_s}{L_d}i_{o,d} + \frac{\omega\, L_q}{L_d}i_{o,q} + \frac{1}{L_d}v_d\,, \tag{3a}$$

$$\frac{\mathrm{d}i_{o,q}(t)}{\mathrm{d}t} = -\frac{R_s}{L_q}i_{o,q} - \frac{\omega\, L_d}{L_q}i_{o,d} - \frac{\omega\,\Psi_{PM}}{L_q} + \frac{1}{L_q}v_q\,, \tag{3b}$$

where L_d (L_q) is the direct (quadrature) axis stator inductance, R_s is the stator resistance, ω is the rotor's angular speed, and Ψ_{PM} denotes the permanent magnet flux. Moreover, v_d and v_q represent the stator voltage vector in the dq frame, respectively. Note that the q component of the output current ($i_{o,q}$) is proportional to the electrical torque, while the d component ($i_{o,d}$) is proportional to the reactive power.

Furthermore, the electromagnetic torque of the PMSM is

$$T_e = \frac{3}{2}\,p[\Psi_{PM}\, i_{o,q} + (L_d - L_q) i_{o,d}\, i_{o,q}]\,, \tag{4}$$

where p is the number of pole pairs of the machine.

C. Continuous-Time Model

The derived equations (1), (2), (3) can be represented by a state-space continuous-time model that defines the different operation modes and states of the BqZSI as follow

$$\frac{\mathrm{d}\boldsymbol{x}(t)}{\mathrm{d}t} = \boldsymbol{F}\boldsymbol{x}(t) + \boldsymbol{G}\boldsymbol{u}_{abc}(t) + d_{\text{aux}_2}\boldsymbol{H}\boldsymbol{w}(t) + \boldsymbol{K}\,, \tag{5a}$$

$$\boldsymbol{y}(t) = \boldsymbol{E}\boldsymbol{x}(t)\,, \tag{5b}$$

where $\boldsymbol{x}(t)$ is the state vector which includes the output dq currents, inductor currents, and capacitor voltages, i.e. $\boldsymbol{x} = [i_{o,d}\; i_{o,q}\; i_{L_1}\; i_{L_2}\; v_{C_1}\; v_{C_2}]^T \in \mathbb{R}^6$. The output dq currents, inductor current, and capacitor voltage compose the output vector, i.e. $\boldsymbol{y} = [i_{o,d}\; i_{o,q}\; i_{L_1}\; v_{C_1}]^T \in \mathbb{R}^4$. In addition, the

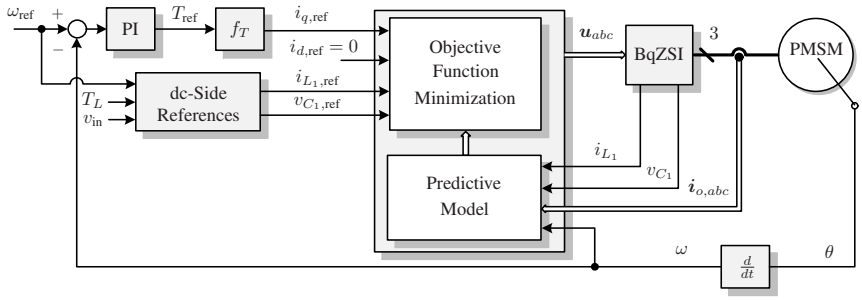

Fig. 4: Proposed MPC scheme for the BqZSI with PMSM.

three-phase switch position $\boldsymbol{u}_{abc} \in \mathcal{U}^3$ represents the system input, i.e. $\boldsymbol{u}_{abc} = [u_a \; u_b \; u_c]^T$ and $\mathcal{U} = \{0, 1\}$. Moreover, $\boldsymbol{w}$ denotes the system disturbance, and it includes the input voltage, i.e. $\boldsymbol{w} = v_{\text{in}} \in \mathbb{R}$. Finally, $\boldsymbol{F} = \boldsymbol{F}_a + d_{\text{aux}_2}\boldsymbol{F}_b$, with

$$\boldsymbol{F}_a = \begin{bmatrix} -\frac{R_s}{L_d} & \frac{\omega L_q}{L_d} & 0 & 0 & 0 & 0 \\ -\frac{\omega L_d}{L_q} & -\frac{R_s}{L_q} & 0 & 0 & 0 & 0 \\ 0 & 0 & 0 & 0 & 0 & 0 \\ 0 & 0 & 0 & 0 & 0 & 0 \\ 0 & 0 & 0 & 0 & 0 & 0 \\ 0 & 0 & 0 & 0 & 0 & 0 \end{bmatrix},$$

$$\boldsymbol{F}_b = \begin{bmatrix} -\frac{R_s}{L_d} & \frac{\omega L_q}{L_d} & 0 & 0 & 0 & 0 \\ -\frac{\omega L_d}{L_q} & -\frac{R_s}{L_q} & 0 & 0 & 0 & 0 \\ 0 & 0 & 0 & 0 & \frac{d_{\text{aux}_1}-1}{L_1} & \frac{d_{\text{aux}_1}}{L_1} \\ 0 & 0 & 0 & 0 & \frac{d_{\text{aux}_1}}{L_2} & \frac{d_{\text{aux}_1}-1}{L_2} \\ \frac{m_1}{C_1} & \frac{m_2}{C_1} & \frac{1-d_{\text{aux}_1}}{C_1} & -\frac{d_{\text{aux}_1}}{C_1} & 0 & 0 \\ \frac{m_1}{C_2} & \frac{m_2}{C_2} & -\frac{d_{\text{aux}_1}}{C_2} & \frac{1-d_{\text{aux}_1}}{C_2} & 0 & 0 \end{bmatrix},$$

and $m_1 = (d_{\text{aux}_1} - 1)\boldsymbol{u}_{abc}^T\boldsymbol{P}_{(:,1)}^{-1}$, $m_2 = (d_{\text{aux}_1} - 1)\boldsymbol{u}_{abc}^T\boldsymbol{P}_{(:,2)}^{-1}$, where $\boldsymbol{P}$ is the Park transformation matrix. Moreover,

$$\boldsymbol{G} = \hat{v}_{\text{dc}} \begin{bmatrix} \frac{1}{L_d} & 0 \\ 0 & \frac{1}{L_q} \\ 0 & 0 \\ 0 & 0 \\ 0 & 0 \\ 0 & 0 \end{bmatrix} \boldsymbol{P}, \quad \boldsymbol{H} = \begin{bmatrix} 0 \\ 0 \\ \frac{1}{L_1} \\ 0 \\ 0 \\ 0 \end{bmatrix},$$

$$\boldsymbol{K} = \begin{bmatrix} -\frac{\omega\Psi_{PM}}{L_q} \\ 0 \\ 0 \\ 0 \\ 0 \\ 0 \end{bmatrix}, \quad \boldsymbol{E} = \begin{bmatrix} 1 & 0 & 0 & 0 & 0 & 0 \\ 0 & 1 & 0 & 0 & 0 & 0 \\ 0 & 0 & 1 & 0 & 0 & 0 \\ 0 & 0 & 0 & 0 & 1 & 0 \end{bmatrix}.$$

where $\hat{v}_{\text{dc}}$ represents the peak dc-link voltage as defined in the appendix in [17]. Moreover, d_{aux_1} and d_{aux_2} are auxiliary binary variables which denote the state and operation mode of the converter, respectively, i.e.

$$d_{\text{aux}_1} = \begin{cases} 0 & \text{if non-shoot-through state} \\ 1 & \text{if shoot-through state} \end{cases}, \tag{6a}$$

$$d_{\text{aux}_2} = \begin{cases} 0 & \text{if buck mode} \\ 1 & \text{if boost mode} \end{cases}, \tag{6b}$$

where the transition from the buck to boost mode (and vice versa) depends on whether the machine speed reference (ω_{ref}) becomes greater (less) than the rated speed (ω_r). When the speed reference is higher than the rated speed, the converter operates in boost mode (the dc-link voltage is boosted to the desired level), otherwise it works in buck mode.

D. Discrete-Time Model

The proposed MPC requires the discrete-model of the system in order to compute the variables predictions. Thus, the continuous-time model (5) is discretized using forward Euler approximation as follows.

$$\boldsymbol{x}(k+1) = \boldsymbol{A}\boldsymbol{x}(k) + \boldsymbol{B}\boldsymbol{u}_{abc}(k) + \boldsymbol{D}\boldsymbol{w}(k) + \boldsymbol{E} \tag{7a}$$

$$\boldsymbol{y}(k) = \boldsymbol{C}\boldsymbol{x}(k), \tag{7b}$$

where $\boldsymbol{A} = (\boldsymbol{F} + \boldsymbol{I})T_s$, $\boldsymbol{B} = \boldsymbol{G}T_s$, $\boldsymbol{D} = \boldsymbol{H}T_s$, $\boldsymbol{E} = \boldsymbol{K}$, and $\boldsymbol{C} = \boldsymbol{E}$. In addition, $\boldsymbol{I}$ is the identity matrix, T_s denotes the sampling interval, and $k \in \mathbb{N}$.

III. Control Scheme

The block diagram of the proposed direct MPC strategy for the BqZSI with PMSM is shown in Fig. 4. The main objective is to control the output dq currents of the machine as well as the capacitor voltage and the inductor current of the dc side of the BqZSI. In addition, the switching frequency is to be kept relatively low in order to reduce the switching losses. The proposed MPC first computes the future trajectories of the controlled variables over a finite prediction horizon based on the system model as well as the measurements of the output current, inductor current, and capacitor voltage. Then, by minimizing the objective function in real time, the optimal switch position for the next time step is chosen.

A. Outer Loops

As can be seen in Fig. 4, based on an outer speed PI control loop, the reference torque is computed. Based on this, the torque-producing current ($i_{q,\text{ref}}$) is calculated using the intermediate function f_T. According to (4), $f_T = \frac{2\,T_{\text{ref}}}{3\,p\,\Psi_{PM}}$. Moreover, the d current is forced to be zero in order to minimize the reactive power, which in turn leads to the torque per ampere optimization.

In order to enable the machine to operate above the rated speed, there are two possibilities. The first scheme is to use a field weakening strategy that results in higher losses. The other is to control the dc-link voltage such that it can be boosted

TABLE I: System Parameters

Parameter	Value
Input voltage v_{in}	24 V
qZS inductances L_1, L_2	500 μH
qZS capacitances C_1, C_2	480 μF
Rated torque T_r	2 Nm
Rated speed ω_r	1000 rpm
d/q-axis inductance L_d/L_q	0.05/0.095 mH
Rotor magnet flux Ψ_{PM}	$7.07e^{-3}$ Wb
Stator resistance R_s	18 mΩ
Number of pole pairs p	5
Sampling interval T_s	20 μs

when the speed increases above the rated speed [19]. With the BqZSI, the dc-link voltage can be adjusted by controlling the capacitor voltage and the inductor current of the BqZS network. Accordingly, the BqZSI operates in the two defined modes of operation; buck mode when the machine speed under the rated speed and boost mode when above the rated speed. In boost mode, the capacitor voltage and inductor current reference values are given by

$$v_{C_1,\text{ref}} = \frac{v_{\text{in}}}{2}(2 + \frac{\omega_{\text{ref}}}{\omega_r}), \quad i_{L_1,\text{ref}} = P_{o,\text{ref}}/v_{\text{in}}, \tag{8}$$

where $P_{o,\text{ref}}$ is the reference output power resulting from the machine speed and load torque ($P_{o,\text{ref}} = \omega T_L \frac{\pi}{30}$).

B. Optimal Control Problem

In order to minimize the error between the reference and the predicted values of the output and the inductor currents, and to control the switching effort, an objective function is formulated as

$$J(k) = ||\boldsymbol{y}_{\text{ref}}(k+1) - \boldsymbol{y}(k+1)||^2_{\boldsymbol{Q}} + \lambda_u ||\Delta \boldsymbol{u}_{abc}(k)||^2. \tag{9}$$

The first term in (9) achieves the output variables tracking, with $\boldsymbol{y}_{\text{ref}} = [i_{o,d,\text{ref}}\ i_{o,q,\text{ref}}\ i_{L_1,\text{ref}}\ v_{C_1,\text{ref}}]^T$. The second term is added to adjust the switching frequency of the qZSI, where $\Delta \boldsymbol{u}_{abc}(k) = \boldsymbol{u}_{abc}(k) - \boldsymbol{u}_{abc}(k-1)$. Moreover, the weighting factor $\lambda_u > 0$ and the diagonal positive semidefinite matrix $\boldsymbol{Q} \in \mathbb{R}^{4\times 4}$ are inserted to set the trade-off between the system performance and the switching effort. Then, by solving the following optimization problem in real time, the optimal solution $\boldsymbol{u}^*_{abc}$ can be obtained

$$\begin{aligned} &\underset{\boldsymbol{u}_{abc}}{\text{minimize}} && J(k) \\ &\text{subject to} && \text{eq. (7)}. \end{aligned} \tag{10}$$

Finally, the resulting optimal switch position is applied to the BqZSI at $k+1$. Similarly, at the next time step, this procedure is repeated with new measurements.

IV. Performance Evaluation

To examine the performance of the proposed MPC with the BqZSI, shown in Fig. 2, simulations were conducted based on MATLAB/Simulink. The system parameters are displayed in Table I. Throughout all the examined cases, the qZSI operates at the desired switching frequency $f_{\text{sw}} = 10$ kHz, by setting $\boldsymbol{Q} = \text{diag}(1, 1, 1, 0.2)$ and appropriately tuning $\lambda_u > 0$ in (9). To achieve a zero steady-state error and good transient response, the parameters of the outer PI control loop are chosen as $K_p = 0.3$ and $K_i = 1.7$.

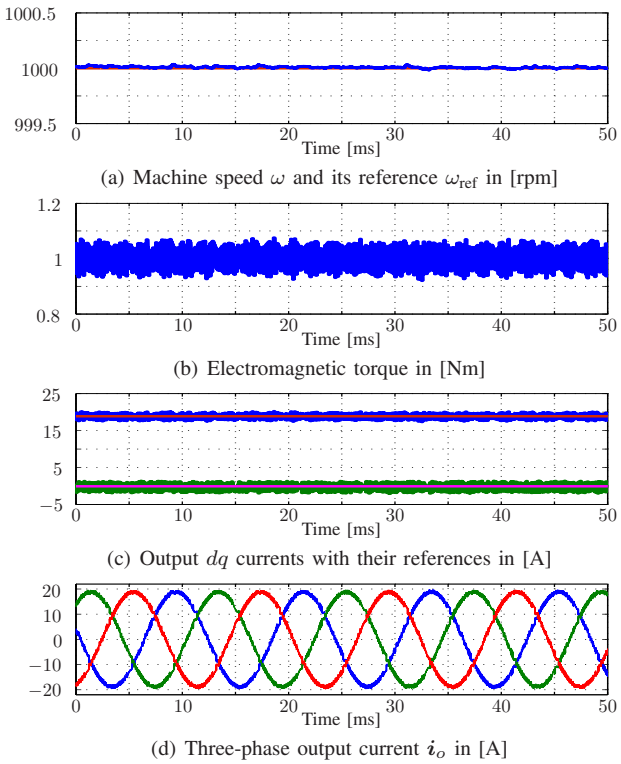

(a) Machine speed ω and its reference ω_{ref} in [rpm]

(b) Electromagnetic torque in [Nm]

(c) Output dq currents with their references in [A]

(d) Three-phase output current $\boldsymbol{i}_o$ in [A]

Fig. 5: Simulation results of the machine side of the qZSI with MPC in buck mode operation. The sampling interval is $T_s = 20\,\mu$s and the switching frequency is $f_{\text{sw}} \approx 10$ kHz.

A. Steady-State Operation

The steady-state behavior of the BqZSI is examined in both modes of operation. In buck mode, the machine works at the rated speed (1000 rpm). The simulation results are shown in Fig. 5. As can be seen, the machine speed effectively tracks its reference at the nominal load torque $T_L = 1$ Nm (see Fig. 5(b)). Moreover, the dq currents are accurately regulated along their reference values (see Fig. 5(c)). The three-phase waveforms of the output current are depicted in Fig. 5(d).

In the second case, the BqZSI is examined when it operates in boost mode, where the speed reference is set to 2000 rpm. The dc- and machine-side results are shown in Figs. 6 and 7, respectively. On the dc side, the capacitor voltage and inductor current perfectly track their references (see Figs. 6(a) and 6(b), respectively), which in turn results in a boosted dc-link voltage as can be seen in Fig. 6(c). As for the machine side, Fig. 7(c) shows that the dq currents are well regulated along their references resulting in a constant machine speed (see Fig. 7(a)). Although the dc side of the BqZSI exhibits a good steady-state behavior, it can be noted that the ripples of the load torque and the dq currents are higher in comparison with the buck mode performance (compare Figs. 5 and 7). The main reason for that is the insertion of the shoot-through states in the boost mode.

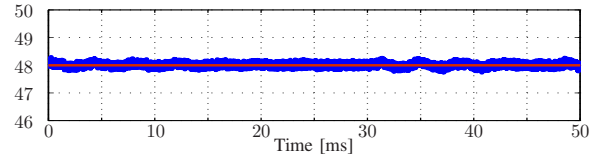

(a) Capacitor voltage v_{C_1} and its reference in [V]

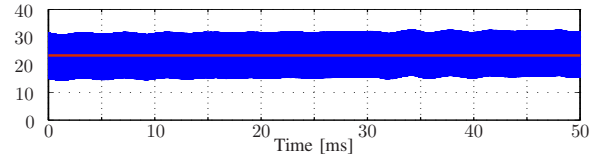

(b) Inductor current i_{L_1} and its reference in [A]

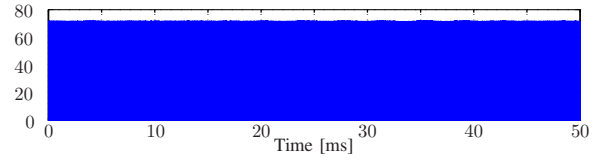

(c) Dc-link voltage v_{dc} in [V]

Fig. 6: Simulation results of the dc side of the qZSI with MPC in boost mode operation.

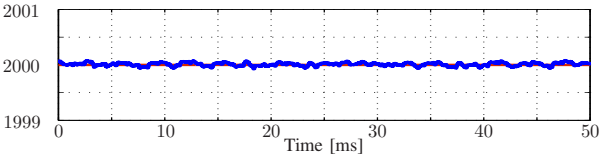

(a) Machine speed ω and its reference ω_{ref} in [rpm]

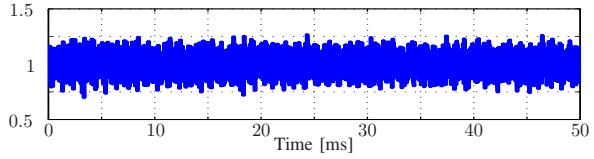

(b) Electromagnetic torque in [Nm]

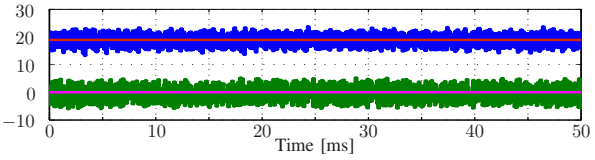

(c) Output dq currents with their references in [A]

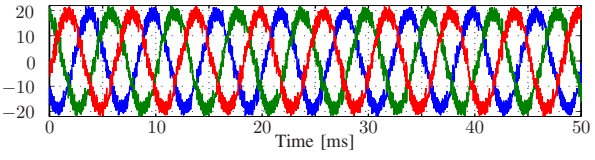

(d) Three-phase output current $\boldsymbol{i}_o$ in [A]

Fig. 7: Simulation results of the machine side of the qZSI with MPC in boost mode operation. The sampling interval is $T_s = 20\,\mu$s and the switching frequency is $f_{\text{sw}} \approx 10$ kHz.

B. Transient Response

The transient performance of the proposed MPC strategy is scrutinized with the BqZSI in two cases: 1) when the BqZSI turns from buck to boost mode under a step change in the speed reference and 2) when the speed reference is reversed.

1) Speed Reference Step Change: In the first case, the speed reference is stepped up from 1000 rpm (buck mode) to 2000 rpm (boost mode). Accordingly, the inductor current

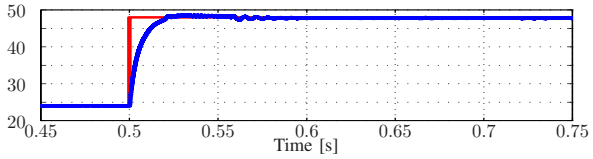

(a) Capacitor voltage v_{C_1} and its reference in [V]

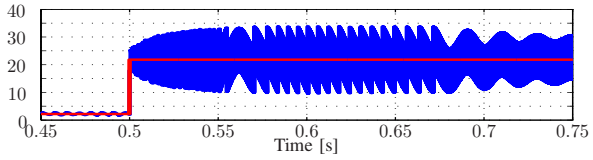

(b) Inductor current i_{L_1} and its reference in [A]

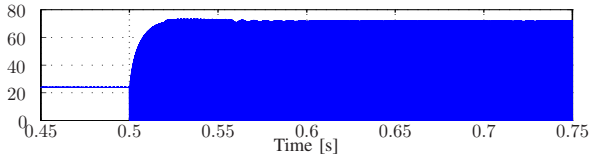

(c) Dc-link voltage v_{dc} in [V]

Fig. 8: Simulation results of the dc side of the qZSI with MPC under a speed reference step change.

reference changes from 2.2 A to 21.8 A, while the capacitor voltage reference is stepped up from 24 V to 48 V (see (8)). The dc- and machine-side results are shown in Figs. 8 and 9, respectively. As can be seen in Fig. 8, the capacitor voltage and inductor current quickly reach their new reference values. Moreover, a zero steady-state error is observed both before and after the transient, i.e. both in buck and boost modes. This is thanks to the discrete-time model of the converter, derived in Section II, which enables the MPC to accurately predict the system behavior over the whole operating regime. As for the machine side, MPC manages to eliminate the speed steady-state error by adjusting the dq currents to their references with a very short transient time (see Figs. 9(a) and 9(c)).

2) Reference Speed Reversal: In the second test, the proposed MPC is investigated under a reversal of the speed reference (from 1000 to -1000 rpm). Since the speed reference is equal to/less than the rated speed, the BqZSI operates at buck mode. The results are displayed in Fig. 10. As can be observed in Fig. 10(a), the speed reference is well tracked, where the MPC achieves a fast tracking for the dq currents (Fig. 10(c)). Moreover, the three-phase currents are reversed when the speed crosses the zero point, see Fig. 10(d).

V. Conclusions

This paper presents a direct MPC strategy to control the BqZSI driving a PMSM for EVs applications. Thanks to the derived model of the system which accurately describes the dynamics of the drive for both buck and boost operating modes, the dq machine currents are simultaneously controlled with the capacitor voltage and inductor current of the dc side over the whole operating range. In order to investigate the performance of the proposed control scheme in steady-state and transient operations, simulation results are presented. The results show that the proposed MPC strategy offers a very good

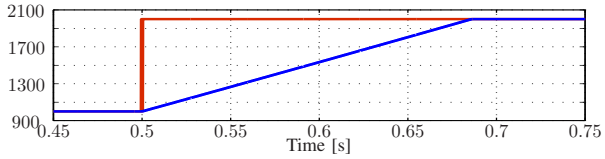

(a) Machine speed ω and its reference ω_{ref} in [rpm]

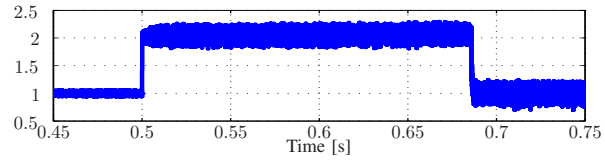

(b) Electromagnetic torque in [Nm]

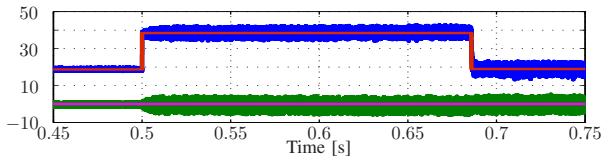

(c) Output dq currents with their references in [A]

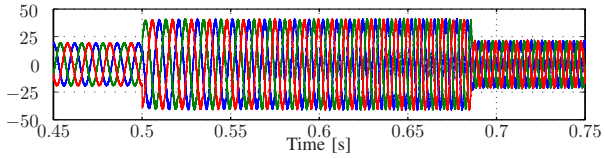

(d) Three-phase output current $\boldsymbol{i}_o$ in [A]

Fig. 9: Simulation results of the machine side of the qZSI with MPC under a speed reference step change.

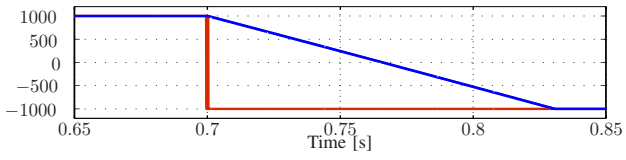

(a) Machine speed ω and its reference ω_{ref} in [rpm]

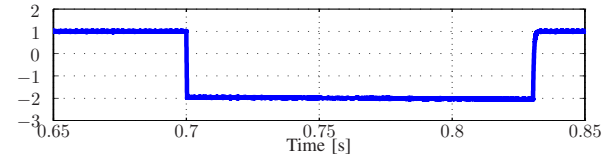

(b) Electromagnetic torque in [Nm]

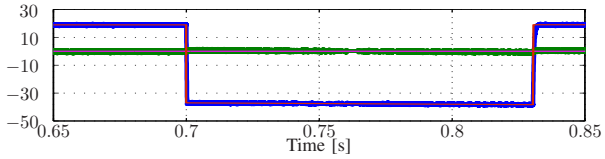

(c) Output dq currents with their references in [A]

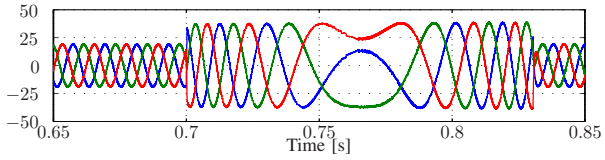

(d) Three-phase output current $\boldsymbol{i}_o$ in [A]

Fig. 10: Simulation results of the machine side of the qZSI with MPC under a speed reversal (from 1000 to -1000 rpm).

steady-state behavior as well as very fast dynamic responses during transients under different operating conditions.

REFERENCES

[1] Z. Zhu and D. Howe, "Electrical machines and drives for electric, hybrid, and fuel cell vehicles," *Proceedings of the IEEE*, vol. 95, no. 4, pp. 746–765, 2007.

[2] K. Chau, C. Chan, and C. Liu, "Overview of permanent-magnet brushless drives for electric and hybrid electric vehicles," *IEEE Trans. Ind. Electron.*, vol. 55, no. 6, pp. 2246–2257, 2008.

[3] A. Battiston, E. H. Miliani, S. Pierfederici, and F. Meibody-Tabar, "Efficiency improvement of a quasi-Z-source inverter-fed permanent-magnet synchronous machine-based electric vehicle," *IEEE Trans. Transport. Electrif.*, vol. 2, no. 1, pp. 14–23, Mar. 2016.

[4] F. Z. Peng, "Z-source inverter," *IEEE Trans. Ind. Appl.*, vol. 39, no. 2, pp. 504–510, 2003.

[5] P. Liu and H. P. Liu, "Permanent-magnet synchronous motor drive system for electric vehicles using bidirectional Z-source inverter," *IET Electric. Systems in Transport.*, vol. 2, no. 4, pp. 178–185, Dec. 2012.

[6] J. Anderson and F. Peng, "Four quasi-Z-source inverters," in *Proc. IEEE Power Electron. Spec. Conf.*, Rhodes, Greece, Jun. 2008, pp. 2743–2749.

[7] Y. Li, S. Jiang, J. Cintron-Rivera, and F. Z. Peng, "Modeling and control of quasi-Z-source inverter for distributed generation applications," *IEEE Trans. Ind. Electron.*, vol. 60, no. 4, pp. 1532–1541, Apr. 2013.

[8] A. Ayad, S. Hanafiah, and R. Kennel, "A comparison of quasi-Z-source inverter and traditional two-stage inverter for PV application," in *Proc. Int. Expo. and Conf. PCIM*, Nuremberg , Germany, May 2015, pp. 1–8.

[9] F. Guo, L. X. Fu, C. H. Lin, C. Li, W. Choi, and J. Wang, "Development of an 85 kW bidirectional quasi-Z-source inverter with DC-link feedforward compensation for electric vehicle applications," *IEEE Trans. Power Electron.*, vol. 28, no. 12, pp. 5477–5488, Dec. 2013.

[10] T. Lannert, A. Welte, T. Gemassmer, and M. Braun, "Control and dynamic performance of the quasi-Z-source-inverter feeding an interior-permanent-magnet-synchronous-machine," in *Proc. Int. Symp. Power Elect., Elect. Drives, Auto. and Motion (SPEEDAM)*, Ischia, 2014, pp. 860–865.

[11] J. Rodríguez, M. P. Kazmierkowski, J. R. Espinoza, P. Zanchetta, H. Abu-Rub, H. A. Young, and C. A. Rojas, "State of the art of finite control set model predictive control in power electronics," *IEEE Trans. Ind. Informat.*, vol. 9, no. 2, pp. 1003–1016, May 2013.

[12] P. Karamanakos, K. Pavlou, and S. Manias, "An enumeration-based model predictive control strategy for the cascaded H-bridge multilevel rectifier," *IEEE Trans. Ind. Electron.*, vol. 61, no. 7, pp. 3480–3489, Jul. 2014.

[13] T. Geyer, G. A. Beccuti, G. Papafotiou, and M. Morari, "Model predictive direct torque control of permanent magnet synchronous motors," in *Proc. IEEE Energy Convers. Cong. and Expo.*, Atlanta, GA, 2010, pp. 199–206.

[14] M. Preindl and S. Bolognani, "Model predictive direct torque control with finite control set for PMSM drive systems, part 1: Maximum torque per ampere operation," *IEEE Trans. Ind. Informatics*, vol. 9, no. 4, pp. 1912–1921, Nov. 2013.

[15] Z. Ma, S. Saeidi, and R. Kennel, "FPGA implementation of model predictive control with constant switching frequency for PMSM drives," *IEEE Trans. Ind. Informatics*, vol. 10, no. 4, pp. 2055–2063, Nov. 2014.

[16] A. Ayad and R. Kennel, "Direct model predictive control of quasi-Z-source inverter compared with the traditional PI-based PWM control," in *Proc. Eur. Power Electron. Conf.*, Geneva, Switzerland, Sep. 2015, pp. 1–9.

[17] A. Ayad, P. Karamanakos, and R. Kennel, "Direct model predictive current control strategy of quasi-Z-source inverters," *IEEE Trans. Power Electron.*, DOI: 10.1109/TPEL.2016.2610459, to appear.

[18] O. Ellabban, H. Abu-Rub, and J. Rodríguez, "Predictive torque control of an induction motor fed by a bidirectional quasi Z-source inverter," in *Proc. IEEE Annual Conf. of IECON*, 2013, pp. 5854–5859.

[19] K. Yamamoto, K. Shinohara, and T. Nagahama, "Characteristics of permanent-magnet synchronous motor driven by pwm inverter with voltage booster," *IEEE Trans. Ind. Appl.*, vol. 40, no. 4, pp. 1145–1152, 2004.